P 3-094

Far Scrape-off Layer Particle and Heat Fluxes in ITER Relevant High Density - High Power Scenarios

H.W. Müller[1,⋆], M. Bernert[1], D. Carralero[1], A. Kallenbach[1], B. Kurzan[1], A. Scarabosio[1], B. Sieglin[1], L. Tophøj[2], N. Vianello[3], E. Wolfrum[1], ASDEX Upgrade Team[1]

[1]*Max-Planck-Institut für Plasmaphysik, Boltzmannstr. 2, D-85748 Garching, Germany*

[2]*Technical University of Denmark, 2800 Lyngby, Denmark*

[3]*Consorzio RFX , Corso Stati Uniti 4, 35127 Padova, Italy*

PACS: 52.55.Fa, 52.55.Rk, 52.55.Ra, 52.25.Fi

PSI-21 keywords: ASDEX-Upgrade, Cross-field transport, Power deposition, Edge Plasma, Probes

⋆ *corresponding author's email: hans.werner.mueller@ipp.mpg.de, phone: ++49 89 3299 1803, fax: ++49 89 3299 2580*

Abstract

The transport across the far scrape-off layer is studied in ASDEX Upgrade for ITER relevant scenarios with high divertor neutral pressure, high power across the separatrix and nitrogen seeding to control the divertor temperature. With high divertor neutral pressure and high power across the separatrix H-mode discharges enter a regime of high cross-field particle and power transport in the far SOL. In this regime parallel particle and power flux densities of several $10^{23}\,\mathrm{m^{-2}s^{-1}}$ and $10\,\mathrm{MWm^{-2}}$ have been detected about $\sim 40{-}45$ mm outside the separatrix mapped to the outer mid-plane. The particle flux fall-off length in this scenario reached up to 45 mm. This paper presents the empirical finding under which conditions this high transport regime appears and delivers a characterisation of the SOL for this regime.

1 Introduction

While in recent years the power fall-off length in the near scrape-off layer (SOL) which determines the peak heat load in the divertor was studied intensively [1] the heat and particle transport across the far SOL to the main chamber first wall still remains an open issue. It is well known that in the far SOL of high density L-mode [2, 3, 4, 5] and H-mode discharges [6] a broad density shoulder forms indicating a large cross-field transport. Previous investigations in L-mode revealed that the density wing formation is related to a change from a conductive to a convective transport regime [3] where also the outer divertor starts to detach and the turbulence characteristic is changing [7, 8]. This agrees well with the model by Myra [9] and Krasheninnikov [10]. This lead to the expectation that a similar transport regime transition will occur in high-density H-modes causing a particle and heat cross-field transport in the far SOL above the values observed in low to medium density H-modes [11]. Therefore, predictions for the particle and heat load of the first wall in ITER require cross-field transport studies in high-density H-modes with an ITER-like SOL. In a previous series of high-density H-mode discharges at a plasma current of $I_p = 1.2\,\mathrm{MA}$, edge safety factor $q_{95} = 3.7$ with ITER relevant SOL parameters and a power across the separatrix of $P_{sep} = P_{heat} - P_{rad} = 4 - 15\,\mathrm{MW}$, with heating power P_{heat} and main chamber plasma radiation P_{rad}, a pronounced density shoulder in the far outboard SOL was

observed when going from a Greenwald fraction of $f_{GW} = 0.5$ to $f_{GW} = 0.7$ [12]. This was accompanied by high parallel heat fluxes $q_{\parallel}$ in the far SOL in the order of several $10\,\mathrm{MWm^{-2}}$ at $dR_{sep,omp} \sim 40\,\mathrm{mm}$ distance to the separatrix mapped to the outer mid-plane. This high cross-field transport regime has now been studied in a systematic way and is presented here.

2 Experimental Set-up and Discharge performance

ASDEX Upgrade is a mid-size divertor tokamak, major radius $R = 1.65\,\mathrm{m}$, minor radius $a = 0.5\,\mathrm{m}$ with the capability to operate at high P_{heat} up to $28\,\mathrm{MW}$ [13]. The maximum achievable $P_{heat}/R \sim 17\,\mathrm{MWm^{-1}}$ and $P_{heat}/R^2 \sim 10\,\mathrm{MWm^{-2}}$ are in the range of the ITER values of $16\,\mathrm{MWm^{-1}}$ and $2.5\,\mathrm{MWm^{-2}}$. The vessel and divertor geometry are similar to the ones planned for ITER with all plasma facing components covered with tungsten. This allows to operate with far SOL and divertor parameters close or even identical to those planned for ITER in terms of plasma-wall clearance ($4 - 10\,\mathrm{cm}$ (mapped to the outer mid-plane), separatrix density $n_{e,sep} = 3 - 4 \times 10^{19}\,\mathrm{m^{-3}}$, density and temperature in the far SOL of $1.5 \times 10^{19}\,\mathrm{m^{-3}}$ and $10\,\mathrm{eV}$, and divertor neutral pressure $p_{0,div} = 1 - 10\,\mathrm{Pa}$ [14, 15].

A fast reciprocating probe (FRP) scans in about $100\,\mathrm{ms}$ a radial distance of $100\,\mathrm{mm}$ at a vertical position $z_{FRP} = 0.312\,\mathrm{m}$ above the vessel mid-plane. The data are sampled with $2\,\mathrm{MHz}$. For the measurements in high power discharges

a Mach type probe head was operated carrying 5 vertically stacked in-plane pins on each side of the probe head and is optimized for high heat loads [16]. The power onto the divertor target is detected by an infra-red ($4.7\,\mu$m) line camera with ~ 3.8 kHz frame rate. The heat flux is derived using the Theodor code [17]. The edge and SOL density profiles at the plasma's outboard side are measured by Thomson scattering [18] with ~ 1.5 mm radial resolution.

The investigation of the H-mode high-transport regime was performed in discharges with $I_p = 1.0$ MA, a magnetic field of $B_t = -2.5$ T where the ion $\nabla B \times B$ drift is directed towards the active lower divertor, and $q_{95} = 4.2$. The plasma was in the so called edge optimized configuration (EOC) where the flux surfaces closely follow the limiter contours. This is a medium triangularity shape with an average $\delta = 0.3$. A typical discharge to study the influence of the line averaged central density $\bar{n}_e$ and the heating power is shown in figure 1. After the ramp up at 2 s a NBI heating power of $P_{NBI} = 7.5$ MW, ECRH in O2-mode with $P_{ECRH} = 1$ MW and ion cyclotron heating with $P_{ICRH} = 1$ MW was injected. The density was varied starting with $\bar{n}_e \approx 0.75 \times 10^{20}\,\mathrm{m}^{-3}$. At 3 s the density was increased to $\bar{n}_e \approx 0.8 \times 10^{20}\,\mathrm{m}^{-3}$ and at 5 s to $\bar{n}_e \approx 0.86 \times 10^{20}\,\mathrm{m}^{-3}$. At 4 s the total heating power P_{heat} was stepped up from 9.5 MW to $P_{heat} = 15$ MW using $P_{NBI} = 12.5$ MW and $P_{ECRH} + P_{ICRH} = 2.5$ MW. P_{sep}/R reached $7.3\,\mathrm{MWm}^{-1}$ and $P_{sep}/R^2 = 4.4\,\mathrm{MWm}^{-2}$, a factor 2 within the ITER values. The applied P_{heat} is the current maximum allowed in ASDEX Upgrade without nitrogen (N_2) seed-

ing to exclude divertor damages. The divertor neutral pressure (1e)), measured under the roof baffle, reaches up to $p_{0,div} = 3.7\,\mathrm{Pa}$ (within the range foreseen for ITER) and the total D puff went as high as $D_{tot} = 6.5 \times 10^{22}\,\mathrm{el/s}$ which corresponds to a divertor neutral density of $N_{0,div} = 9.3 \times 10^{22}\,\mathrm{m}^{-3}$ (1c). As visible from the divertor shunt current measurement (figure 1f) the outer divertor remains attached throughout. Here we like to point out that T_{div} is an approximation of the divertor temperature derived from the shunt current [19]. The H-factor in #30732 stays about constant at $H_{98,y2} = 0.74 - 0.8$. Nevertheless, with the highest applied gas puff there is a slight decrease in the stored energy (figure 1d)) indicating that the discharge starts to enter the degrading H-mode regime [20]. In the analysis of the cross-field transport no obvious effect of the H-mode degradation was found so far in comparison with non-degrading discharges.

The effect of the N_2 seeding and divertor detachment was investigated in a second discharge series where it was tried to keep the density constant at $\bar{n}_e \approx 0.86 \times 10^{20}\,\mathrm{m}^{-3}$ with $P_{heat} = 15\,\mathrm{MW}$. In these discharges first N_2 was seeded with feedback control to reach $T_{div} = 20, 10, 5\,\mathrm{eV}$ in steps and finally a strong feed forward N_2 puff of $N_{tot} = 3.9 \times 1022\,\mathrm{el/s}$ was applied to achieve divertor detachment. An example is presented in figure 2. With N_2 seeding no indication of a degrading H-mode was seen. With increasing N_2 puff $N_{0,div}$ decreases. Albeit the N partial pressure is underestimated by a factor 2.5 this effect is expected to be below $15\,\%$ for $N_{0,div}$ due to the low N concentration. At about $5.5\,\mathrm{s}$ T_{div} becomes

negative which indicates that the outer divertor completely detaches.

3 Entering the high cross-field transport regime

Figure 3a) shows time averaged ($0.6-1.0$ s time average depending on the plateau period) edge and SOL density profiles from the Thomson scattering diagnostic for the various density and heating power plateaus in #30733 which was almost identical to #30732. The data outside ~ 40 mm are not very reliable due to strong scatter. With increasing density a broad shoulder with $n_e > 10^{19}$ m^{-3} forms across the SOL - the same density as expected in ITER - while the $n_{e,sep}$ reaches up to 2.9×10^{19} m^{-3}. Between the profiles taken at 2.9 and 4.1 s, P_{heat} went up from 9.5 MW to 15 MW, while between 5.5 s and 6.5 s the mixture of P_{ECRH} and P_{ICRH} was changed, see figure 1b). Both variations in the heating scheme do not significantly affect the density profile. At a distance $dR_{sep,mag} \approx 47$ mm a swept Langmuir probe facing towards the outer divertor shows $n_e = 0.6-1.6\times10^{19}$ m^{-3} for the different density steps.

In figure 3b) the ion saturation current I_{sat} detected by a Langmuir probe on the FRP is shown for the three density steps in #30732. The probe is located at $dR_{sep,FRP} \approx 55$ mm and facing towards the outer divertor. As an ELM monitor the bolometer signal of a diode observing the divertor entrance at 500 kHz sampling rate is presented in figure 3c). At 2.3 s and $\bar{n}_e \approx 0.75 \times 10^{20}$ m^{-3}

there is a weak inter-ELM I_{sat} signal only. With $\bar{n}_e \approx 0.8 \times 10^{20}\,\mathrm{m}^{-3}$ and $P_{heat} = 15\,\mathrm{MW}$ at $4.8\,\mathrm{s}$ the ELMs become longer. Also in between the ELMs the I_{sat} probe detects density blobs or filaments - even when no activity is detected by the bolometers at the divertor entrance. Finally at $\bar{n}_e \approx 0.85 \times 10^{20}\,\mathrm{m}^{-3}$ the Langmuir probe shows a continuous stream of filaments at $2 - 3\,\mathrm{kHz}$. The time averaged parallel current density at the Langmuir probe - including ELM and inter-ELM intervals - rises from $\bar{j}_{sat} = 25 - 30\,\mathrm{kAm}^{-2}$ to $55 - 60\,\mathrm{kAm}^{-2}$ and finally reaches $\bar{j}_{sat} = 80 - 85\,\mathrm{kAm}^{-2}$. This is an increase by a factor of about 3 while the density varies by $15\,\%$ only. The strong rise in $\bar{j}_{sat}$ already starts between $\bar{n}_e \approx 0.75 \times 10^{20}\,\mathrm{m}^{-3}$ and $\bar{n}_e \approx 0.8 \times 10^{20}\,\mathrm{m}^{-3}$ before the H-mode begins to degrade.

The particle flux into the outer divertor increases with density. While the temperature profile stays almost unchanged the divertor electron density rises. The electron temperature profile is shifted outward with respect to the peak particle flux indicating that the divertor is in the high recycling regime. The power profile in the outer divertor (figure 3d)) shows a strong increase in the deposited power with $\bar{n}_e$ when going from 0.75 to $0.8 \times 10^{20}\,\mathrm{m}^{-3}$. From $2.9\,\mathrm{s}$ to $4.1\,\mathrm{s}$ the power step of P_{heat} is visible. A final increase in the deposited power occurs with the next density step to $\bar{n}_e = 0.85 \times 10^{20}\,\mathrm{m}^{-3}$. In the logarithmic plot the broadening of the power density profile with increasing $\bar{n}_e$ becomes well visible.

The observed $\bar{j}_{sat}$ and profile evolutions with density show that there exists a

regime with high cross-field particle transport. The density shoulder formation and related $\bar{j}_{sat}$ increase is equivalent to the transition from the conductive to the convective (high cross-field) transport regime in L-mode [7]. Enlarging the data base by the $1.2\,$MA discharges from last campaign presented in [12], $0.8\,$MA discharges at high Greenwald fraction f_{GW} in EOC configuration with $P_{heat} = 7.5 - 10\,$MW as well as ITER baseline scenario discharges at $I_p = 1.1\,$MA and $P_{heat} = 5 - 7.5\,$MW with high density and f_{GW}, high $\delta \approx 0.4$ and low $q_{95} = 3.6$ shows neither $\bar{n}_e$ nor f_{GW} are satisfying ordering parameters for the occurrence of the high-transport regime in H-mode. This can be shown when plotting $\bar{j}_{sat}$, which is a measure for the amount of cross-field transport, versus f_{GW} (figure 4a)) or $\bar{n}_e$ figure 4b). Even at high $\bar{n}_e$, $\bar{j}_{sat}$ can be rather low in the far SOL. The presented $\bar{j}_{sat}$ measurements are performed at $dR_{sep,FRP} = 54 - 58\,$mm at $z_{FRP} = 0.312\,$m. To obtain a more appropriate empirical ordering parameter for the occurrence of the high transport regime a reduced data set is used where $\bar{n}_e$, P_{sep} and $dR_{sep,FRP}$ are almost constant but $\bar{j}_{sat}$ changes strongly. This is found in discharge #30736, a N_2 seeded discharge, with $\bar{n}_e = 0.84 - 0.89 \times 10^{20}\,\mathrm{m}^{-3}$ while $\bar{j}_{sat} = 36 - 84\,\mathrm{kAm}^{-2}$ varies strongly. The distance to the separatrix is $dR_{sep,FRP} = 58 - 68\,$mm. As presented in figure 2 N_2 seeding causes a strong variation in $N_{0,div}$. In fact $N_{0,div}$ is a good ordering parameter as shown in figure 5a). Not only $\bar{j}_{sat}$ from the N_2 seeded discharge (shown in red) line up but also $\bar{j}_{sat}$ from the density scan in #30733 (marked in orange). For the latter outliers occur

at high $N_{0,div}$. The most obvious ones can be related to a low P_{sep}. To verify this assumption the data set of figure 5a) is plotted in 5b) as function of $N_{0,div} \times P_{sep}$ which shows a stronger scatter but less outliers. This ordering parameter is applied to the whole data set of figure 4a) and b) and presented in figure 6a). $N_{0,div} \times P_{sep}$ is a satisfying ordering parameter for the whole data set. At highest $N_{0,div} \times P_{sep}$, $\bar{j}_{sat}$ seems to saturate which is not yet validated, e.g. a higher P_{sep}, which was not achieved so far, might allow for a higher $\bar{j}_{sat}$. So far our analysis does not reveal a relation between divertor (partial) detachment and the onset of the high transport regime.

The underlying physical mechanism to access the high transport regime has not been identified yet. Nevertheless, it is obvious that $N_{0,div}$ which is proportional to the $p_{0,div}$ is a key element to enter the high transport regime in H-mode. A second player is P_{sep}. A sufficiently high P_{sep} is required to obtain a high $\bar{j}_{sat}$ in the far SOL.

4 Features of the high cross-field transport regime

As already shown, the high transport regime is accompanied by a high filament frequency in the far SOL and a high $\bar{j}_{sat}$ up to $90\,\mathrm{kAm}^{-2}$ at $dR_{sep,FRP} \approx 55\,\mathrm{mm}$ which corresponds to $dR_{sep,omp} \approx 40 - 50\,\mathrm{mm}$ in the outer mid-plane. $\bar{j}_{sat}$ can be related to a parallel heat flux density via $q_{\parallel} = j_{sat}/e(\gamma k_B T_e + E_{rec})$ where e is the

elementary charge, γ the sheath transmission factor, T_e the electron temperature and $E_{rec} = 13.6\,\text{eV}$ the recombination energy of Deuterium. In #30732 a swept single probe delivers mean electron temperatures of $17.9, 16.1$ and $15.3\,\text{eV}$ - in ITER $10\,\text{eV}$ are expected - for the time intervals shown in figure 3b) with $\bar{n}_e = 0.75\times10^{20}\text{m}^{-3}$, $\bar{n}_e = 0.75\times10^{20}\text{m}^{-3}$ at $P_{sep} \approx 10\,\text{MW}$, and $\bar{n}_e = 0.85\times10^{20}\text{m}^{-3}$. Assuming a typical $T_i/T_e = 2$ and a secondary electron emission coefficient of 0.25 [21] we get $\gamma = 9.1$. This results in particle and heat fluxe densities of $\Gamma_{parallel} = 1.9, 3.8, 5.3 \times 10^{23}\,\text{m}^{-2}\text{s}^{-1}$ and $q_{\|} = 5.3, 9.6, 13.0\,\text{MWm}^{-2}$. Here one has to keep in mind that with a realistic maximum inclination angle between B-field and surface normal of $87\,\text{deg}$ the flux density perpendicular to the wall $q_{\perp}$ is at most a factor 20 lower than $q_{\|}$. It is likely that the heat flux derived from the probe measurements even underestimates $q_{\|}$ by a factor $2-3$ as observed in [12]. Taking into account that parts of the ITER first wall can handle $q_{\perp} = 2\,\text{MWm}^{-2}$ only [15] and ITER has to operate at high $p_{0,div}$ and P_{sep}, this calls for further investigation.

Using $N_{0,div} \times P_{sep}$ to sort the data sets into different categories the fall-off length of $\bar{j}_{sat}$ (λ_j) can be determined as shown in figure 6b). For $N_{0,div} \times P_{sep} = 10 - 20 \times 10^{26}\,\text{Wm}^{-3}$ $\lambda_j = 10\,\text{mm}$ and rises as expected to $\lambda_j = 45 - 47\,\text{mm}$ for $N_{0,div} \times P_{sep} = 90 - 110 \times 10^{26}\,\text{Wm}^{-3}$ again indicating the strongly enhanced cross-field particle transport.

5 Discussion and Summary

In H-mode a regime exists with high cross-field transport in the far SOL. In ASDEX Upgrade this regime is entered at high $N_{0,div}$ and P_{sep}. It is empirically found that the high transport sets in at $N_{0,div} \times P_{sep} > 20 \times 10^{26}\,\mathrm{Wm}^{-3}$. Investigations in L-mode discharges at ASDEX Upgrade [7] lead to the interpretation that an increase of the effective collisionality $\Lambda = L_c v_{ei} \Omega_i / (c_s \Omega_e)$ causes a change in the filamentary transport from conduction to convection dominated for $\Lambda > 1$ - caused by different closure conditions for the parallel current [10]. This provokes a high cross-field transport at the outer midplane [9]. Here, L_c is the connection length, v_{ei} the electron-ion collision frequency, c_s the ion sound speed and Ω_i, Ω_e the ion and electron gyrofrequency. Assuming similar SOL densities and temperatures in the SOL of ITER as in ASDEX Upgrade, which is likely for inter-ELM periods while unknown during ELMs, $\Lambda > 1$ is more likely in ITER due to a larger $L_c(ITER) \approx 2L_c(AUG)$. In Alcator C-Mod, which has a much smaller wall clearance, the high transport regime has been related to a main chamber recycling regime [3, 22].

In the high transport regime particle fluxes up to $\Gamma_\parallel = 5.3 \times 10^{23}\,\mathrm{m}^{-2}\mathrm{s}^{-1}$ and heat fluxes up to $q_\parallel = 13.0\,\mathrm{MWm}^{-2}$ are found at $dR_{sep,FRP} \approx 55\,\mathrm{mm}$ which maps to $dR_{sep,omp} = 40 - 50\,\mathrm{mm}$. λ_j of up to 47 mm was measured at z_{FRP}. In a convection dominated transport regime λ_q will have a similar value.

Albeit a high $N_{0,div}$ is required to reach the high transport regime in H-mode with the divertor in the high recycling regime points towards a similarity to the L-mode behavior further data analysis and experiments are required to identify the underlying physical processes determining the transport regime in H-mode as well as to improve the predictive capability for the SOL cross-field transport in ITER and DEMO. Especially an ELM resolved analysis is necessary and a predictive model for the filament creation is needed.

Acknowledgement

This project has received funding from the European Union's Horizon 2020 research and innovation programme under grant agreement number 633053. The views and opinions expressed herein do not necessarily reflect those of the European Commission.

References

[1] T. Eich et al., J. Nucl. Mater. **438** (2013) S72.

[2] N. Asakura, et al., J. Nucl. Mater. **241-243** (1997) 559.

[3] B. LaBombard, et al., Phys. Plasmas **8** (2001) 2107.

[4] D.L. Rudakov et al., Nucl. Fusion **45** (2005) 1589.

[5] O.E. Garcia, et al., Plasma Phys. Control. Fusion **48** (2006) L1.

[6] J. Neuhauser, et al., Plasma Phys. Control. Fusion **44** (2002) 855.

[7] D. Carralero, et al., accepted Nucl. Fusion.

[8] D. Carralero, et al., this conference.

[9] J.R. Myra, et al., Phys. Plasmas bf 13 (2006) 112502.

[10] S.I. Krasheninnikov, et al., J. Plasma Physics **74** (2008) 679.

[11] A. Herrmann et al., Plasma Phys. Control. Fusion **46** (2004) 971.

[12] H.W. Müller, et al., to be published.

[13] A. Herrmann, O. Gruber, Fusion Science and Technology **44** (2003) 569.

[14] R.A. Pitts, et al., Phys. Scr. **T138** (2009) 014001.

[15] R.A. Pitts, et al., J. Nucl. Mater. **415** (2011) S957.

[16] H.W. Müller, et al., Nucl. Fusion (2011) **51** (2011) 073023.

[17] A. Herrmann et al., Plasma Phys. Control. Fusion **37** (1995) 17.

[18] B. Kurzan, et al., Plasma Phys. Control. Fusion **46** (2004) 299.

[19] A. Kallenbach et al., Plasma Phys. Control. Fusion **52** (2010) 055002.

[20] M. Bernert, Plasma Phys. Control. Fusion, in preparation

[21] M.E. Woods et al., J. Phys. D: Appl. Phys. **20** (1987) 1136.

[22] M.V. Umansky, et al., Phys. Plasmas **5** (1998) 3373.

Figure captions

Figure 1:

Discharge parameters for a density scan. Shown are a) I_p (black), $\bar{n}_e$ (blue), f_{GW} (green), b) P_{heat} (red) and P_{rad} (orange), c) $N_{0,div}$ (blue), D_{tot} (black) and N_{tot} (red), d) stored energy W_{mhd} (black) and H-factor (blue), e) $p_{0,div}$ from an ionisation gauge below the baffle (black) and a baratron behind the inner divertor (blue), f) divertor shunt current $I_{shunt,out}$ (black) and FRP stroke position (red).

Figure 2:

Discharge parameters for a N_2 seeding scan. a) I_p (black), $\bar{n}_e$ (blue), f_{GW} (green) and FRP stroke position (bordeaux), b) heating power and P_{rad} (orange), c) $N_{0,div}$ (blue), D_{tot} (black) and N_2 puff (red)), d) W_{mhd} (black), H-factor (blue) and $I_{shunt,out}$ (bordeaux), e) T_{div} (red) and requested divertor temperature (black), f) $p_{0,div}$ from a ionisation gauge (black) and a baratron (blue).

Figure 3:

a) Edge n_e profiles from the Thomson scattering diagnostic for different $\bar{n}_e$. b) I_{sat} measurements at $dR_{sep,FRP} \approx 55$ mm for different $\bar{n}_e$ in #30732 and c) line integrated bolometer signal from the divertor entrance at the same time periods. d) Power density profile in the outer divertor plotted over the target surface coordinate.

Figure 4:

a) $\bar{j}_{sat}$ *in dependence of* f_{GW} *for different discharge scenarios. All measurements are made in the range* $dR_{sep,FRP} = 54 - 58\,mm$. *b) The same data set plotted over* $\bar{n}_e$.

Figure 5:

a) $\bar{j}_{sat}$ *from a discharge with* N_2 *seeding (red diamonds) and a* $\bar{n}_e$ *scan (orange horizontal hour glasses) as function of* $N_{0,div}$ *at* $dR_{sep,FRP} = 58 - 68\,mm$. *b) The same data plotted over* $N_{0,div} \times P_{sep}$.

Figure 6:

a) Data set from figure 4a) plotted over $N_{0,div} \times P_{sep}$. *b)* $\bar{j}_{sat}$ *in dependence of* $dR_{sep,FRP}$ *for different* $N_{0,div} \times P_{sep}$ *ranges.*

figures

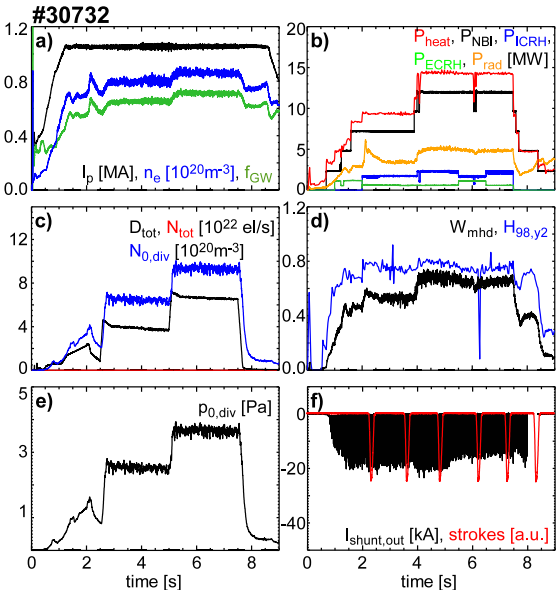

Figure 1:

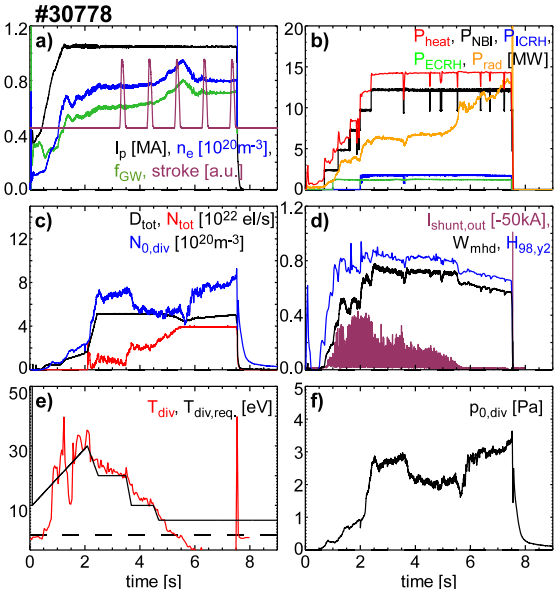
#30778
a)
I_p [MA], n_e [10^{20}m^{-3}],
f_{GW}, stroke [a.u.]
b)
P_{heat}, P_{NBI}, P_{ICRH},
P_{ECRH}, P_{rad} [MW]
c)
D_{tot}, N_{tot} [10^{22} el/s]
$N_{0,div}$ [10^{20}m^{-3}]
d)
$I_{shunt,out}$ [-50kA],
W_{mhd}, $H_{98,y2}$
e)
T_{div}, $T_{div,req}$, [eV]
f)
$p_{0,div}$ [Pa]
time [s]
time [s]

Figure 2:

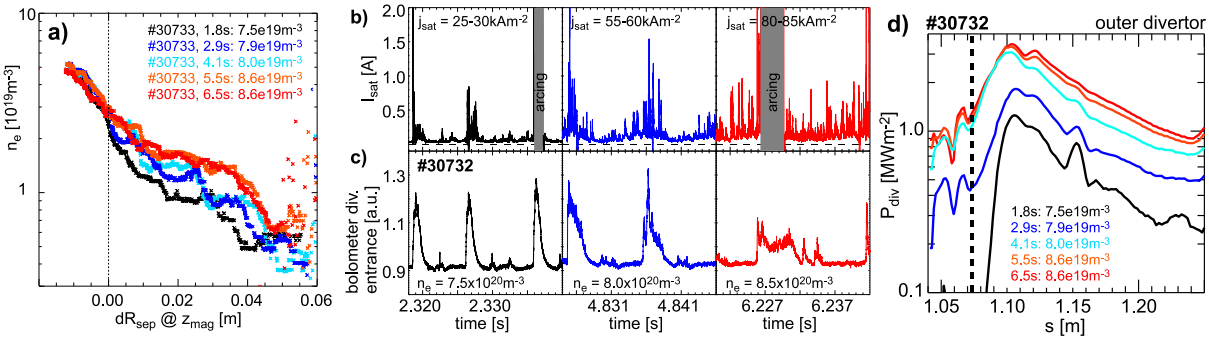
a)
#30733, 1.8s: 7.5e19m-3
#30733, 2.9s: 7.9e19m-3
#30733, 4.1s: 8.0e19m-3
#30733, 5.5s: 8.6e19m-3
#30733, 6.5s: 8.6e19m-3
ne [10^19m-3]
dRsep @ zmag [m]
b)
jsat = 25-30kAm-2
jsat = 55-60kAm-2
jsat = 80-85kAm-2
arcing
Isat [A]
c)
#30732
bolometer div. entrance [a.u.]
ne = 7.5x10^20m-3
ne = 8.0x10^20m-3
ne = 8.5x10^20m-3
time [s]
d)
#30732
outer divertor
Pdiv [MWm-2]
1.8s: 7.5e19m-3
2.9s: 7.9e19m-3
4.1s: 8.0e19m-3
5.5s: 8.6e19m-3
6.5s: 8.6e19m-3
s [m]

Figure 3:

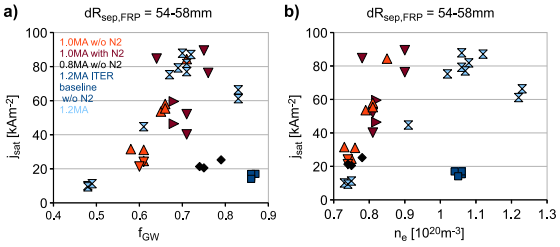
a)
dR$_{sep,FRP}$ = 54-58mm
1.0MA w/o N2
1.0MA with N2
0.8MA w/o N2
1.2MA ITER baseline -w/o N2
1.2MA
j$_{sat}$ [kAm^{-2}]
f$_{GW}$
b)
dR$_{sep,FRP}$ = 54-58mm
j$_{sat}$ [kAm^{-2}]
n$_e$ [10^{20}m^{-3}]

Figure 4:

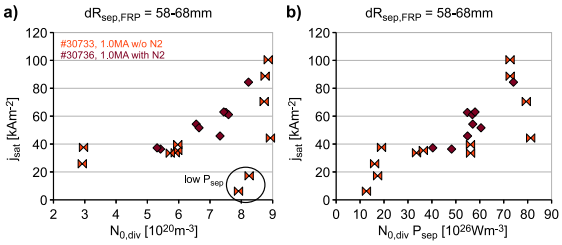
a)
dR$_{sep,FRP}$ = 58-68mm
#30733, 1.0MA w/o N2
#30736, 1.0MA with N2
low P$_{sep}$
j$_{sat}$ [kAm^{-2}]
N$_{0,div}$ [10^{20}m^{-3}]
b)
dR$_{sep,FRP}$ = 58-68mm
j$_{sat}$ [kAm^{-2}]
N$_{0,div}$ P$_{sep}$ [10^{26}Wm^{-3}]

Figure 5:

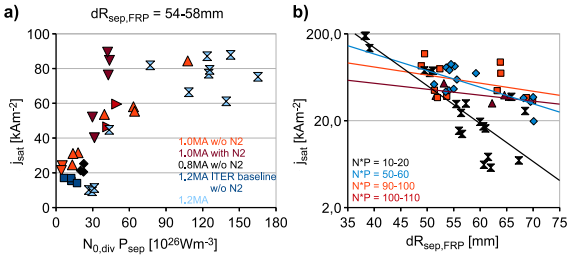
a)
dR$_{sep,FRP}$ = 54-58mm
100
80
60
40
20
0
j$_{sat}$ [kAm^{-2}]
0
30
60
90
120
150
180
N$_{0,div}$ P$_{sep}$ [10^{26}Wm^{-3}]
1.0MA w/o N2
1.0MA with N2
0.8MA w/o N2
1.2MA ITER baseline
w/o N2
1.2MA
b)
200,0
20,0
2,0
j$_{sat}$ [kAm^{-2}]
35
40
45
50
55
60
65
70
75
dR$_{sep,FRP}$ [mm]
N*P = 10-20
N*P = 50-60
N*P = 90-100
N*P = 100-110

Figure 6: